Progress In Electromagnetics Research, PIER 24, 201–225, 1999

A GENERALIZED FINITE SIZED DIPOLE MODEL FOR RADAR AND MEDICAL IMAGING PART I: NEAR FIELD FORMULATION FOR RADAR IMAGING

T. S. Naveendra

RF and Radios Division
CET Technologies Pte Ltd.,
Singapore Technologies Electronics,
Singapore Technologies Building,
Singapore 609602

P. R. P. Hoole

Division of Communications Engineering,
School of Electrical and Electronic Engineering
Nanyang Avenue, Block S1,
Nanyang Technological University
Singapore 639798

1. Introduction
2. Review of Radar Imaging Techniques
2.1 Resolution Criterion
2.1.1 Range Resolution
2.1.2 Azimuth Resolution
2.2 Synthetic Aperture Radar (SAR)
2.2.1 SAR Theory (Unfocused Aperture)
2.2.2 SAR Theory (Focused Aperture)
3. Electric Dipole Based Back Scattered Signal Model
3.1 Magnitude Modifying Factor
3.2 Phase Modifying Factor
3.3 Near-Electric Field Based Imaging
3.3.1 Electromagnetic Wave Transmission
3.3.2 Electromagnetic Wave Reflection
3.3.3 Signal Processing

4. Near Field Imaging Results
4.1 Radial Component (E_r) Based Imaging
4.2 Tangential Component (E_θ) Based Imaging
4.3 Imaging Based on Resultant of E_r and E_θ
5. Correction for Modifying Factors
5.1 Magnitude Modifying Factor
5.2 Phase Modifying Factor
6. Conclusions
References

1. INTRODUCTION

Ever since Heinrich Hertz demonstrated the basic Radar principle, numerous civil and military applications have been developed. Out of these, Radar imagery has been in the forefront of the emerging Radar technology. Here radar signals are transmitted and by appropriate processing of the signals reflected from targets, images are formed [1]. Soon it was realized that images of high resolution were required for the more demanding requirements such as target identification, terrain mapping and terrain characterization. The conventional Radar was incapable of delivering such high-resolution images due to several practical limitations. This led to the development of the concept of Synthetic Aperture Radar (SAR). Maps created with SAR techniques are near photographic in quality. In these maps information is conveyed by the contrast in brightness from one point to another. Bright spots represent stronger radar signal reflection. The strength of radar returns depend on the slope of the scene as seen by the radar, the roughness of the surface as gauged by the wavelength of the radio signal in use and on the electrical properties of the surface material. Sensitivity to roughness and slope also vary with frequency and polarization of the electromagnetic signal [1]. Thus it is seen that the quality of the image obtained and the depth of information it conveys depend heavily on the electromagnetic signal properties. Hence there is impetus for looking more closely at the signal models used in the imaging process.

It has been noted that conventional SAR imaging routines usually assume a far-field electromagnetic signal in modeling the reflected radar signals [2, 3]. By modeling the reflected signals encompassing the near-electromagnetic fields, new insights could be gained with regard to SAR images. This has been attempted in this paper. In this regard

an electric dipole based signal model has been used. Another aspect scrutinized is the influence of target material properties. The reflected signal properties are changed according to the material properties of the target. Although this effect is seen to be less significant on the image [3], it is characterized in the proposed signal model. Recently there have been attempts at computing the Radar Cross Sections (RCS) of targets in a laboratory environment using a spherical wave near field formulation [4]. At typical indoor distances the effect of the near electromagnetic fields is pronounced and correction for this effect has to be incorporated at some stage of the reconstruction process. Failure to do so will account for inaccurate calculation of the RCS of the target. In [5] the misrepresentation of image domain data has been directly related to incorrect computation of RCS. The RCS can be calculated from image domain data if the scatterers are independent and non-directional. In practice the scatterers do not satisfy these conditions. A new term called 'scattering brightness' has been introduced instead of RCS in [5]. Since the elemental dipoles have a near isotropic radiation pattern and can be considered as independent scatterers, the images obtained using the method proposed in this paper could be used for RCS calculation in the near-field region.

In section 2 a brief review of the SAR imaging principles has been presented. An electric dipole based signal model incorporating the near electromagnetic fields for the scattered radar data is presented in section 3. The effects of the distant—dependent near electromagnetic fields on the magnitude and phase of the received signals are characterized by the introduction of two factors, namely, *Magnitude Modifying Factor (MMF)* and *Phase Modifying Factor (PMF).* Image reconstruction results using the orthogonal electric fields present in the near-field region is given in section 4. It is seen that these images do not convey the reflectivity information accurately. A correction to overcome this effect is proposed and implemented in section 5. In section 6 some conclusions are drawn.

2. REVIEW OF RADAR IMAGING TECHNIQUES

Radar imagery creates maps or images of large areas of terrain. Radar signals are transmitted as pulses and based on the information relayed to the radar system by the echoes, images are created. Some of the basic concepts and principles of radar imaging are presented in this section.

2.1 Resolution Criterion

Resolution is defined as the minimum distance by which two points on the ground could be separated and still be discerned individually by the radar. This is illustrated in Fig. 2.1 where a side looking radar is shown.

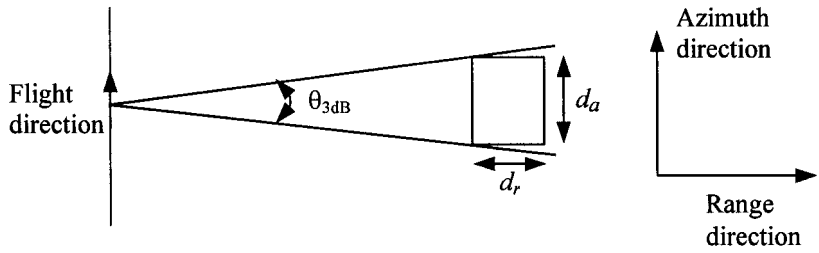

Figure 2.1. Side looking radar beam and resolution.

2.1.1 Range Resolution

To resolve two scatterers in the range direction the target separation must be such that the trailing edge of the transmitted pulse should have passed the near target before the leading edge of the echo from the far target reaches the near target [3, 6, 7].

Say it takes T_1 and T_2 seconds for the echoes to return from the near and far targets at d and $(d + \Delta)$ respectively. Hence we get

$$T_1 = \frac{2d}{c} \qquad T_2 = \frac{2(d+\Delta)}{c}$$

For the imaging system to discern the two targets, it must be able to resolve the time difference of

$$T_2 - T_1 = \tau = \frac{2\Delta}{c}$$

Therefore, in terms of distance, the resolution is characterized by

$$d_r = \frac{c\tau}{2} \tag{2.1}$$

where d_r is the range resolution limit.

2.1.2 Azimuth Resolution

In general fine resolution is obtained more readily in range rather than in the azimuth direction. To discern two targets in the azimuth direction, they should be separated by at least the 3 dB beamwidth of the antenna in the azimuth direction times the range of the target from the radar. Thus the azimuth resolution at range R is given by

$$d_a = R\phi_{3dB} \tag{2.2}$$

To get fine azimuth resolution, as seen from (2.2) that the 3 dB beamwidth of the radar antenna should be reduced by some means. This could be achieved using the concept of Synthetic Aperture Radar.

2.2 Synthetic Aperture Radar (SAR)

Synthetic Aperture Radar (SAR) is an airborne radar mapping technique for generating high-resolution maps. Azimuth resolution is increased in SAR by coherently integrating echo energy reflected from the ground or targets as the aircraft carrying the radar flies past the radar illuminated area/target to be mapped.

2.2.1 SAR Theory (Unfocused Aperture)

Fig. 2.2 shows the geometry used for generating a synthetic aperture. A synthetic aperture of length L is generated by an airborne radar platform flying along the indicated path from $-vT/2$ to $+vT/2$, where v is the platform velocity relative to the ground and T is the total time within which data is collected (integration time) [1].

Point targets are shown at boresight and at a displacement of y along cross range direction. Targets are illuminated for a time determined by radar range R, aircraft velocity v and the real antenna aperture beamwidth. Time t is taken to be zero when the aircraft is at the minimum range R to the point target at $y = 0$. A range variation of δR exist before and after $t = 0$.

The echo signal phase at each position along the synthetic aperture is the two-way phase relative to the transmission phase. The two-way phase advance of an echo from $y = 0$ is [1]

$$\Psi_1(t) = -\frac{4\pi}{\lambda}\frac{v^2 t^t}{2R} \tag{2.3}$$

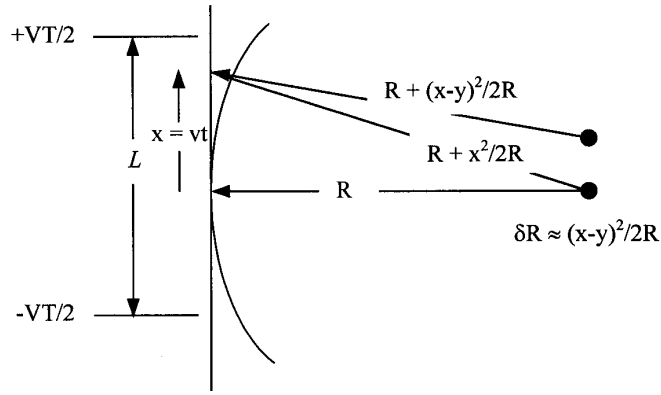

Figure 2.2 Geometry for generating a synthetic aperture.

This is a quadratic phase term resulting from straight-line motion of the platform past the scene to be mapped. Unfocused SAR results when this phase term is not corrected for at the signal processing stage.

The two way phase advance of an echo signal from a point target at position y is

$$\Psi_2(t,y) = -\frac{\frac{4\pi}{\lambda}(x-y)^2}{2R} \tag{2.4}$$

where $x = vt$. Assuming the pulse frequency to be high enough, the echoes are integrated in the time interval $-T/2$ to $+T/2$.

$$Z(y) = \int_{-T/2}^{+T/2} \exp\left[-\frac{j4\pi}{2R\lambda}(vt-y)^2\right] dt$$

The power response is thus given by [1]

$$|Z(y)|^2 = \left\{\int_{-T/2}^{+T/2} \cos\left[\frac{2\pi}{R\lambda}(vt-y)^2\right] dt\right\}^2 + \left\{\int_{-T/2}^{+T/2} \sin\left[\frac{2\pi}{R\lambda}(vt-y)^2\right] dt\right\}^2 \tag{2.5}$$

Power gain response of the unfocused synthetic aperture, when normalized to peak gain at $y = 0$, can be expressed in terms of Fresnel integrals as [1]

$$\frac{|Z(y)|^2}{|Z(0)|^2} = \frac{T^2\left(\frac{R\lambda}{4v^2T^2}\right)\left\{[C(\eta-\zeta)-C(\eta+\zeta)]^2+[S(\eta-\zeta)-S(\eta+\zeta)]^2\right\}}{T^2\left(\frac{R\lambda}{4v^2T^2}\right)[4C^2(\eta)+4S^2(\eta)]}$$

$$= \frac{[C(\eta-\zeta)+C(\eta+\zeta)]^2+[S(\eta-\zeta)+S(\eta+\zeta)]^2}{4[C^2(\eta)+S^2(\eta)]} \tag{2.6}$$

where $\eta = \frac{vT}{\sqrt{R\lambda}}$ and $\zeta = \frac{2y}{\sqrt{R\lambda}}$. The power gain response is maximized at the peak of the response to a target at $y = 0$, when $C^2(\eta) + S^2(\eta)$ is maximum. From the plots of the Fresnel integrals, it was found that this occurs at $\eta \approx 1.2$. Thus the peak power response to a point target occurs when $\eta = 1.2 = \frac{vT}{\sqrt{R\lambda}}$. Therefore the optimum unfocused aperture length corresponding to $\eta \approx 1.2$ is

$$L = vT \approx 1.2\sqrt{R\lambda} \tag{2.7}$$

The half-power resolution corresponding to this length is found by solving for the value of ζ that satisfies $\left|\frac{Z(\phi)}{Z(0)}\right|^2 = 0.5$ at $\eta = 1.2$. A graphical solution gives $\zeta = 0.5$ as the answer. Hence the resolution d_a is given by

$$d_a = 2|y| = \zeta\sqrt{R\lambda} = 0.5\sqrt{R\lambda} \tag{2.8}$$

It is seen from (2.8) that the resolution degrades as the square root of range and wavelength. Focusing is employed to remove the dependence of the azimuth resolution on range and wavelength.

2.2.2 SAR Theory (Focused Aperture)

The quadratic phase term $\Psi_1(t)$ in (2.3), produced by the straight-line motion of the radar platform, can be subtracted from the total phase $\Psi_2(t)$ to generate a focused aperture. Therefore the corrected two-way phase term is [1]

$$\Psi_2(t,y) - \Psi_1(t) = -\frac{\frac{4\pi}{\lambda}(x-y)^2}{2R} - \left(-\frac{\frac{4\pi}{\lambda}x^2}{2R}\right) = \frac{4\pi}{\lambda}\left(-\frac{xy}{R}+\frac{y^2}{2R}\right) \tag{2.9}$$

where $x = v.t.$ The normalized radar response versus cross range distance from boresight y becomes [1]

$$\frac{|Z(y)|^2}{|Z(0)|^2} = \frac{\sin^2\left(\dfrac{2\pi vTy}{R\lambda}\right)}{\left(\dfrac{2\pi vTy}{R\lambda}\right)^2} \tag{2.10}$$

To find the half-power points of the focused synthetic aperture of length $L = vT$, the above expression is set equal to 0.5. We get $\frac{2\pi vTy}{R\lambda} = \pm 1.39$. Therefore

$$y|_{3\,dB} = \pm 0.22\frac{R\lambda}{L} \tag{2.11}$$

Hence the resolution measured at half-power points is

$$d_a = 0.44\frac{R\lambda}{L} \tag{2.12}$$

It is seen that the resolution is better in this instance when compared to unfocused SAR. Further using (2.2) and the expression for the beamwidth of the antenna $\phi|_{3\,dB} = 0.88\frac{\lambda}{l}$, the azimuth resolution becomes

$$d_c = \frac{0.44R\lambda}{0.88R\frac{\lambda}{l}} = \frac{l}{2} \tag{2.13}$$

Hence the resolution in the cross range is independent of range and wavelength. It is seen that smaller the dimension of the antenna in the cross range direction, better the azimuth resolution.

From the above analysis it is evident that focused aperture processing gives rise to images with better resolution and independent of the range and frequency involved. This is achieved by removing the quadratic phase term due to the straight-line motion of the radar platform from the received signals. This step will not be necessary if the platform is moving in a circular path over the terrain to be imaged [3]. There are problems associated with focusing due to an inability to calculate the relative velocity between radar and target accurately and erroneous calculation of the distance to the center of the region to be imaged. These errors are corrected using techniques described in [8, 9].

In imaging routines the effect of the near electromagnetic fields are not properly taken into account. The far-field assumption is valid

when imaging targets at very large distances, typically in the kilometer range. But this assumption breaks down when imaging is performed in confined regions at distances of up to a few meters. This is particularly true in instances where imaging is done by illuminating targets in an anechoic chamber and subsequently using the image domain data to calculate RCS values. In the near field region orthogonal field components are present [10] and this complicates matters further. Hence a study of the electromagnetic fields in the near and far field regions is imperative for a better understanding of the images formed in the near field region.

3. ELECTRIC DIPOLE BASED BACK SCATTERED SIGNAL MODEL

Radar signals are transmitted through free space as electromagnetic waves and are composed of orthogonal electric and magnetic fields. The radar return signal strength is determined by the reflection (scattering) mechanism of the electromagnetic fields impinging on the target. If the distance to the scatterer is large compared to the wavelength and antenna dimension, the incident field could be considered to be in the far field zone of the antenna. This enables the incident field to be considered as a spherical wave front rather than a plane wave [11, 12]. A closer look at the reflection mechanism will reveal the following:

i. On incident at the surface, the electric/magnetic fields induce localized fields and hence electric and magnetic currents on the surface. The currents induced will be influenced by the material properties. The material properties will determine the re-radiated signal magnitude and phase change.
ii. These currents which are proportional to the incident field strengths, re-radiate electromagnetic fields at the original frequency of the signal. These current elements could thus be modeled by infinitesimal electric dipoles. Since the scatterers can be modeled by elemental electric dipoles, the electric field components at a receiver in the near-field region of these dipoles are the radial and tangential components given by [10]

$$E_r = A\left[\frac{1}{r^2} + \frac{1}{jkr^3}\right] e^{-jkr} \tag{3.1}$$

$$E_\theta = jA\left[\frac{1}{r} + \frac{1}{jkr^2} - \frac{1}{k^2r^3}\right] e^{-jkr} \tag{3.2}$$

where the factor A could be found using techniques described in [11], k is the wave-number and r is the distance between scatterer and transceiver.

If the receiving antenna is close to the scatterer or the size of the antenna is large compared to the distance from the target, the antenna will be in the near field zone of the scatterer. This makes the analysis difficult. Alternatively, the discrete induced current elements could be considered separately. This allows the electromagnetic field elements to be considered as belonging to the far field zone and expressed as a spherical wave. This simplifies the analysis. The received signal is the coherent summation of the individual radiation signals from the infinitesimal radiating elements [11]. Here the distances from the radiating elements to the receiver are all different. This is in contrast to the far field analysis where the distance is considered equal and very large compared to the antenna dimensions and wavelength. Based on these observations a near field spherical wave illumination radar imaging algorithm has been developed.

In the near field region the received signal strength is a function of the distance of the transceiver from the scatterer elements. Moreover it will be shown that the received signal magnitude varies as a function of distance as dictated by the *Magnitude Modifying Factor (MMF)* and that the phase information is corrupted by a *Phase Modifying Factor (PMF).*

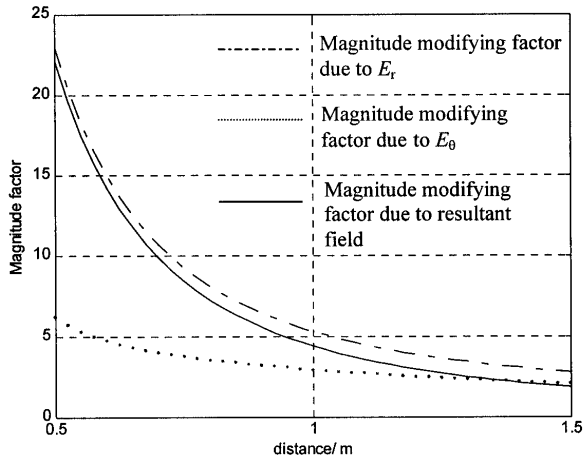

Figure 3.1 Variation of magnitude modifying factor.

3.1 Magnitude Modifying Factor

Depending on whether the receiver picks up the radial, tangential or the circularly polarized summation of these two orthogonal fields, the return radar signals will be modulated by the following *MMFs* respectively:

$$F_R(r) = A\left(\frac{1}{r^4} + \frac{1}{k^2 r^6}\right)^{1/2} \tag{3.3}$$

$$F_\theta(r) = A\left(\frac{1}{r^2} - \frac{1}{k^2 r^4} + \frac{1}{k^4 r^6}\right)^{1/2} \tag{3.4}$$

$$F(r) = \sqrt{F_R^2 + F_\theta^2} \tag{3.5}$$

The variation of these factors with distance is shown in Fig. 3.1.

The MMFs related to E_r, E_θ and the resultant field are plotted in Fig. 3.1. The range of distance used here to compute the MMFs correspond to applications in near field radar imaging, near-field RCS measurements and biomedical imaging. The variation of the MMF due to E_r is rapid in the region of 0.5-1.0 m. A difference in distance of a few tens of centimeters between two identical scattering cross sections will modify the scattered signal strength between the two surfaces by a factor of two or more. Comparatively, the variation of the MMF due to E_θ is not rapid and the degree of change is not marked. The variation of the resultant $(\sqrt{F_r^2 + F_\theta^2})$ closely resembles the variation of E_r . Since the paper explores the possibility of imaging with E_r, E_θ and $\sqrt{F_r^2 + F_\theta^2}$, the later being the term used in existing imaging technology, all three modifying factors are included in the SAR imaging algorithms proposed.

3.2 Phase Modifying Factor

Due to the complex nature of the electromagnetic signals in the near field region they give rise to a distance dependent phase angle. This has been termed the *Phase Modifying Factor (PMF).* This factor is given by (3.6) and (3.7) when the back scattered signals are modeled by E_r and E_θ respectively.

$$\phi_r = \tan^{-1}\left(-\frac{1}{kr}\right) \tag{3.6}$$

$$\phi_\theta = \tan^{-1}\left(\frac{k^2r^2 - 1}{kr}\right) \tag{3.7}$$

The variation of this additional phase angle shift is shown in Fig. 3.2.

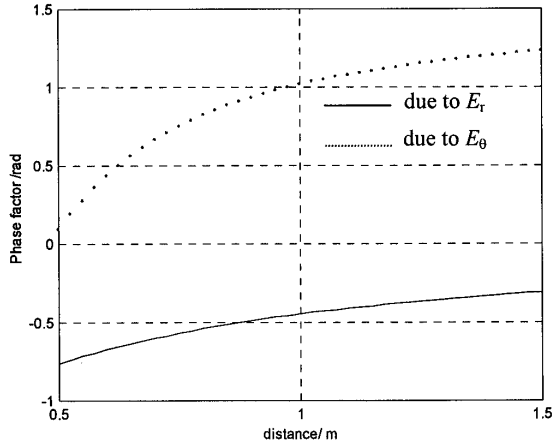

Figure 3.2 Variation of the phase modifying factor.

The variation of the PMF associated with E_θ is more pronounced than that of E_r . In SAR and MRI the phase information is important [8, 9, 13, 14]. Knowledge of the underlying signal model will help in evaluating the additional phase angle shift and correcting for it.

3.3 Near-Electric Field Based Imaging

Conventional SAR imaging algorithms assume a far field approximation of the reflected radar return signals [2, 6, 7]. This assumption is true for very far distances as defined by

$$r < \frac{2{D_{eff}}^2}{\lambda} \tag{3.8}$$

where D_{eff} is the effective aperture of the source antenna/element and λ is the wavelength. D_{eff} is the dimension of a real aperture, which would give the same beamwidth as the synthetic aperture. But the analysis in section 3.1 and 3.2 shows:

i. The received electric field strength depends on the scatterer distance from the receiver.
ii. The field strength and phase information changes are different in the case of E_r and E_θ.

Therefore, if imaging is done in the near field region, images created using conventional signal processing algorithms will not produce images which represent the true nature of the imaged region or object. In order to determine the effect of using E_r and E_θ field components of the re-radiated electromagnetic wave in the near field region for imaging, a series of simulation studies were carried out. Each step of the imaging process is explained and the relevant results are presented.

3.3.1 Electromagnetic Wave Transmission

Linearly frequency modulated sinusoids are transmitted as pulses from the radar transmitting antenna. These chirp signals can be written using complex notation as

$$s(t) = e^{j(2\pi f_c t + 0.5at^2)}; \qquad 0 \le t \le \tau \tag{3.9}$$

where a is termed the chirp rate and τ is the pulse width. Functions of this form are used since they compress into very sharp autocorrelations and offers a higher signal bandwidth. A wide bandwidth is required for high resolution images since the image is actually a narrowband reconstruction of the reflectivity function of the target [2].

3.3.2 Electromagnetic Wave Reflection

The transmitted electromagnetic waves reflect off the target and the return echoes will have only a fraction of the amplitude transmitted. The return echoes can be expressed as

$$r(t - t_d) = \sigma F(r) e^{j\left(2\pi f_c \overline{t-t_d} + 0.5a\overline{t-t_d}^2 + \phi + \theta\right)}; \quad 0 \le t - t_d \le \tau \tag{3.10}$$

where t_d is the round trip time delay of the signal in reaching the receiver, σ is the scattering coefficient of the scatterer, $F(r)$ the *Magnitude Modifying Factor,* ϕ is the phase angle due to the *Phase Modifying Factor* and θ is the phase angle due to complex impedance of the scatterer.

The scattering coefficient σ will depend on the angle of incidence of the electromagnetic signal, frequency, polarization and on the electrical

properties of the scatterer. Since the scatterer will have finite value of conductivity, scatterers are usually not purely dielectric and have complex impedance given by [10]

$$Z = \sqrt{\frac{j\omega\mu}{\sigma + j\omega\varepsilon}} \tag{3.11}$$

where ω is the radian frequency of the signal, μ the permeability and ε the permittivity of the material. The reflection coefficient of a material, that has impedance of Z_2 is defined as [10]

$$\rho_{R,E}\angle\theta = \frac{Z_2 - Z_1}{Z_2 + Z_1} \tag{3.12}$$

where Z_1 is the impedance of the free space, and it is approximately equal to 120π. The reflected signal $r(t)$ is given by

$$r(t) = \rho_{R,E}\angle\theta.s(t) \tag{3.13}$$

Thus, it is seen that when electromagnetic signals are scattered from objects that have complex impedance, the objects introduce a phase shift to the reflected signal. The effect of this complex impedance phase angle on the autocorrelation function is shown in Fig. 3.3.

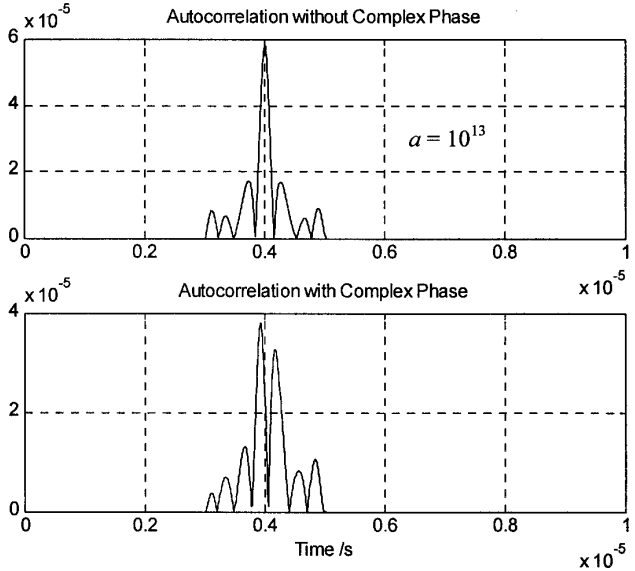

Figure 3.3 Autocorrelation without and with complex impedance phase angle.

It is seen from Fig. 3.3 that when the return signal is corrupted with the complex impedance phase angle, the peak of the autocorrelation function shifts position and the sidelobe levels also increase. In this example the shift was found to be 7×10^{-8} s at a chirp rate $a = 10^{12}$. This corresponds to a misposition of the scatterer by about 21 m in the range bins. This will lead to image distortion. This effect, may get lumped together with the image artifacts introduced due to 2D relative translation motion between receiver and scatterer [15]. This phase shift is seen to decrease when the chirp rate is increased. For example when the chirp rate was increased to 10^{13} the corresponding shift of the peak was reduced to 1×10^{-8} seconds. A correction to alleviate this effect is presented in section 5.2.

3.3.3 Signal Processing

In order to extract the phase information without ambiguity, quadrature demodulation followed by matched filtering is employed [2].

(a) Quadrature Demodulation

A reference signal

$$ref(t) = \cos(2\pi f_{ref} t).rect\left(\frac{t}{\tau}\right); \qquad 0 \leq t \leq \tau \tag{3.14}$$

is used in the demodulation process which frequency down converts the return signal to a more manageable intermediate frequency f_{IF} given by

$$f_{IF} = f_c - f_{ref} \tag{3.15}$$

The low-pass filter output will be

$$r_{if}(t) = \sigma e^{j[2\pi(f_{IF}t - f_c t_d) + 0.5a(t-t_d)^2 + \theta]}.rect\left(\frac{t-t_d}{\tau}\right) \tag{3.16}$$

(b) Matched Filtering (Range Compression)

Taking the return signal to be corrupted by Additive White Gaussian Noise (AWGN), the optimum filter to compress the signal is the Matched Filter [2]. This has the advantage that it gives maximum SNR and also holds on to the phase information. This filter can be implemented as a correlation of the two functions, a time reversed linear filter or a conjugate frequency domain receiver [1]. Therefore the

reference signal for matched filtering is

$$u(t) = e^{j[2\pi(f_i f t + 0.5at^2)]}.rect\left(\frac{t}{\tau}\right) \tag{3.17}$$

The matched filter output can be written as

$$\begin{aligned} y(t) &= \int u^*(s)r(s+t)ds = \sigma \int u^*(s)u(s+t-t_d)ds \\ &= \sigma A(t-t_d) \end{aligned} \tag{3.18}$$

where $A(t)$ is the autocorrelation of the signal $u(t)$ and is given by

$$A(t) = \Phi.(\tau - |t|).\frac{\sin\left[\pi at(\tau - t)\right]}{\pi at(\tau - t)} \tag{3.19}$$

where Φ is the unit magnitude phase contribution which includes θ, and $(\tau - |t|)$ is a weighting function which changes the magnitude of the sinc function.

If there are N re-radiating sources, $r(t)$ will be given by

$$r(t) = \sum_{i=i}^{N} \sigma_i u(t - \tau_i) \tag{3.20}$$

The output of the correlation receiver will be

$$\begin{aligned} y(t) &= \int u^*(s)r(s+t)ds \\ &= \sum_{i=1}^{N} \sigma_i A(t - \tau_i) \end{aligned} \tag{3.21}$$

Thus, the matched filter output is the time-shifted version of the autocorrelation of the reference signal. It is seen that the transmitted pulse has been compressed after reception to yield better resolution. Following every transmission the return from each resolvable range increment, dictated by the chirp pulse parameters, is added to the contents of the appropriate range bin. This builds up a range compressed data matrix A.

In order to illustrate the principles behind near field imaging, three scattering points were used and the return or reflection data is collected

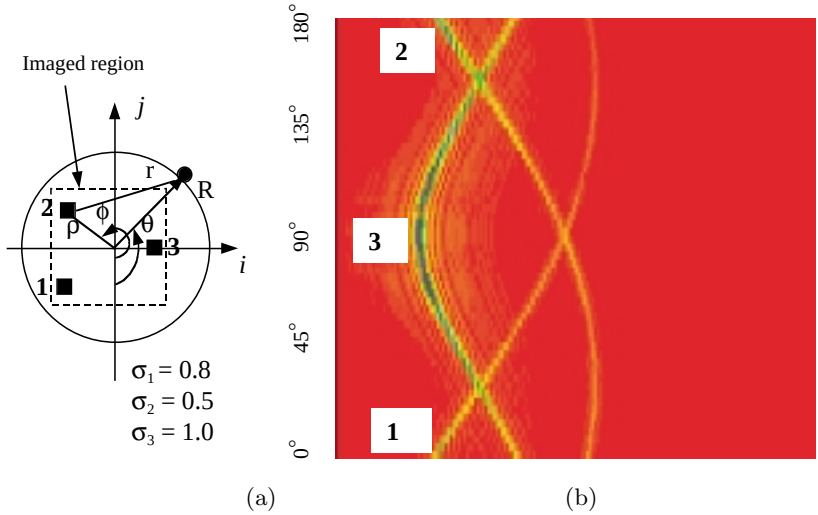

(a) (b)

Figure 3.4 (a) Data collection arrangement, (b) Range compressed data.

in a circular path as shown in Fig. 3.4(a). In the imaging routine, SAR concepts have been used. Since data collection was done in a circular path, it is inherently a focused synthetic aperture approach with no additional steps for focusing required [3]. The range-compressed data is shown in Fig. 3.4(b). These are sinograms, which satisfy

$$f(i,j) \equiv r^2 = R^2 + \rho^2 - 2R\rho\cos(\phi - \theta) \tag{3.22}$$

Signals are collected at N points along the circular path in the interval $0 \leq \theta \leq 180°$. The signals collected at each point are range compressed and stored in the corresponding range bins. The range r and the corresponding time delay t_d are related by

$$t_d = r/c \tag{3.23}$$

where c is the velocity of the electromagnetic wave in free space. Assuming a sampling time of t_s, the position of the bin n corresponding to a time delay t_d is given by

$$n = t_d/t_s \tag{3.24}$$

The following points could be noted from the range compressed data (sinograms) which have been numbered corresponding to the scatterers as shown in Fig. 3.4(b).

i. Signal data from a single scatterer is spread in different range bins for different positions of the sensor. This is called range migration [2].
ii. The received signal strength for one scatterer varies along the corresponding sinogram. This is apparent from the intensity variation along each of the sinograms. This is due to the *Magnitude Modifying Factor* (associated with E_r in the example shown) which modulates the received signal strength according to the distance of the scatterer from the different positions of the sensor.
iii. Scatterer reflectivity is not correctly represented in the sinograms. In the example, scatterers 1 and 3 have been assigned a reflectivity of 0.8, 1.0 respectively. Hence, the intensity profile of the corresponding sinograms should also reflect that ratio. But it is evident from the figure that it is not so. This discrepancy is also attributable to the effect of the *Magnitude Modifying Factor.*

Since the range compressed data is used in the subsequent imaging steps, the effect due to the near field MMF is reflected in the final image obtained after azimuth compression.

(c) Azimuth Compression

For different positions of the receiver, the range and thus the time delay (bin position) for a single scatterer will change as shown in Fig. 3.4(b). To get the final image, the spread of energy of a single scatterer in different range bins should be added together. This process is known as azimuth compression [2].

Azimuth compression is done by integrating along each sinogram and assigning the sum to the correct position in the image plane [16]. Let the region to be imaged; shown in Fig. 3.4(a), be divided into N by N resolution cells. The intensity in any cell represented by $I(p,q)$ can be written as

$$I(p,q) = \sum_{j=1}^{N} \sum_{i=1}^{N} \delta(i - n_{pq}) A_{ij}; \qquad p,q = 1 \ldots N \tag{3.25}$$

where A_{ij} is the range compressed data matrix and n_{pq} is defined as $n_{pq} = t_{dpq}/ts$. Time delay t_{dpq} corresponds to the time taken for a signal from a scatterer at position corresponding to a point denoted by p and q in the image plane, to get to the reference point.

4. NEAR FIELD IMAGING RESULTS

4.1 Radial Component (E_r) Based Imaging

If the sensor is aligned in such a way so as to receive the radial component E_r of the re-radiated electromagnetic waves, the received signal strength will be a function of the *Magnitude Modifying Factor* $F_R(r)$. The return signal could be modeled by

$$r(t - t_d) = \sigma F_R(r) e^{j\left(2\pi f_c \overline{t-t_d} + 0.5a\overline{t-t_d}^2 + \theta + \phi\right)} \tag{4.1}$$

Following the imaging procedure described in section 3, the image of the test case of three scatterers is as shown in Fig. 4.1.

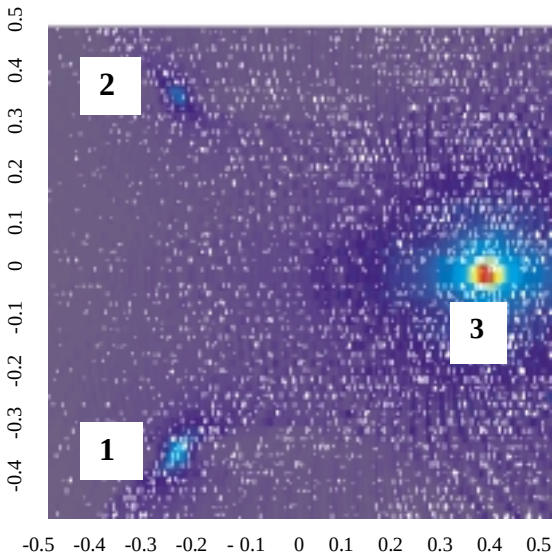

Figure 4.1 E_r based image of the three scatterers.

It is seen that the intensity of scatterer-3 is very high compared to that of scatterers 1 and 2. The intensities are not in proportion to the assigned scattering coefficients of 1.0, 0.8 and 0.5 respectively. This is due to the *Magnitude Modifying Factor* $F_R(r)$, the variation of which is shown in Fig. 3.1. The scatterer reflecting property has been misrepresented on the image. This will lead to incorrect values of RCS unless the function $F(r)$ is properly accounted for in the image

synthesis algorithm. The error in image intensity across the image plane is high as 28 dB. This amount of variation will make the image useless for statistical studies, segmentation, etc.

4.2 Tangential Component (E_θ) Based Imaging

In this case the received signal strength will be a function of the *Magnitude Modifying Factor* $F_\theta(r)$. The return signal will be given by

$$r(t - t_d) = \sigma F_\theta(r) e^{j\left(2\pi f_c \overline{t-t_d} + 0.5a\overline{t-t_d}^2 + \theta + \phi\right)} \tag{4.2}$$

The image obtained with this signal model will be as shown in Fig. 4.2. The scatterer intensity variation is not high as in the case of imaging with E_r. The difference in the relative values of intensity of scatterers is less when the tangential component of the electric field E_θ is used in the imaging process. But the image is not accurate in representing the reflectivity data on the image. The error in intensity in the image plane is around 10-12 dB.

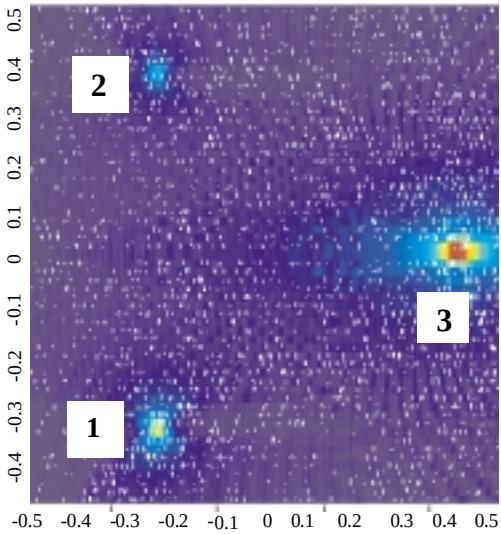

Figure 4.2 E_θ based image of the three scatterers.

4.3 Imaging Based on Resultant of E_r and E_θ

If the signal due to the resultant of E_r and E_θ (circularly polarized) is used the signal model will be

$$r(t-t_d) = \sigma\sqrt{F_R(r)^2 + F_\theta(r)^2}\, e^{j\left(2\pi f_c \overline{t-t_d} + 0.5a\overline{t-t_d}^2 + \phi\right)} \tag{4.3}$$

The image obtained with a signal model as given in (4.3) will be as shown in Fig. 4.3. The image does not represent the reflectivity data correctly. The error in intensity in the image plane is found to be around 15 dB. The complete magnitude-modifying factor is dominated by the factor due to E_r. This is apparent by comparing the graphs in Fig. 3.1, where the variation due to E_r is more rapid and intense than due to E_θ.

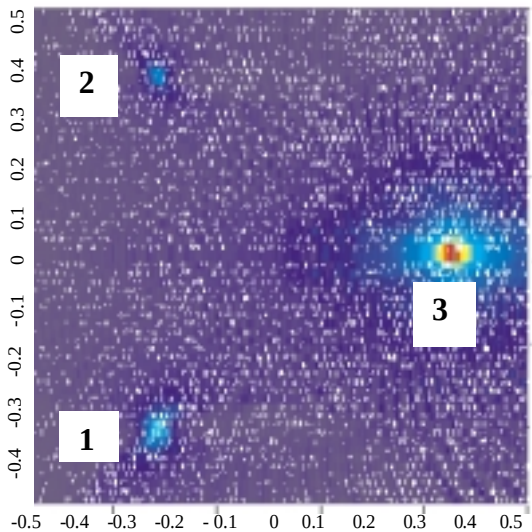

Figure 4.3 Image based on resultant of E_r and E_θ.

5. CORRECTION FOR MODIFYING FACTORS

5.1 Magnitude Modifying Factor

The signals received from different points in the region to be imaged are modulated to different values by the *Magnitude Modifying Factor.*

To eliminate this effect, the data received has to be corrected before going on to the image synthesis stage. The correction proposed here is introduced to the range compressed data.

The bin n_{ij} in the range-compressed data matrix A corresponds to the distance r_j between a scatterer and the transceiver at a particular time instant. The relationship between n_{ij} and r_j could be written as

$$r_j = n_{ij}.t_s.u \tag{5.1}$$

where t_s is the sampling time, u the velocity of the radio waves and i, j denotes the row and column number of matrix A respectively. The row number in turn is equal to the number of observation points of the transceiver. Since the distance involved with each bin is known the *Magnitude Modifying Factor* for the data in a particular range bin could be calculated and the entire column of the range-compressed data matrix corrected by the correction factor $F(r_j)$. Correction factors for each column could be computed and the data corrected prior to azimuth compression. This suppresses the effect due to the near field *Magnitude Modifying Factor* on the image. A column of the corrected range compressed data matrix $A'(:, j)$ could be obtained by

$$A'(:, j) = \frac{A(:, j)}{F(r_j)} \tag{5.2}$$

where j denotes the column number and : denotes all rows.

For imaging with the tangential field component E_θ the image obtained after imposing this correction is shown in Fig. 5.1.

It is seen that the image in Fig. 5.1 represents the reflectivity data accurately after the correction has been incorporated into the imaging routine. Similar correction was applied to images obtained with E_r and the resultant field and the true image was obtained. Thus, it is imperative that the correction for *Magnitude Modifying Factor* be included when imaging in the near field region.

5.2 Phase Modifying Factor

It was shown in section 3.3.2, that the peak of the autocorrelation function is shifted due to the *Phase Modifying Factor.* It was also seen that the shift reduces when the chirp rate was increased. In the imaging scenario considered the chirp rate used was 10^{15}. The effect of the *Phase Modifying Factor* was found imperceptible on the images synthesized.

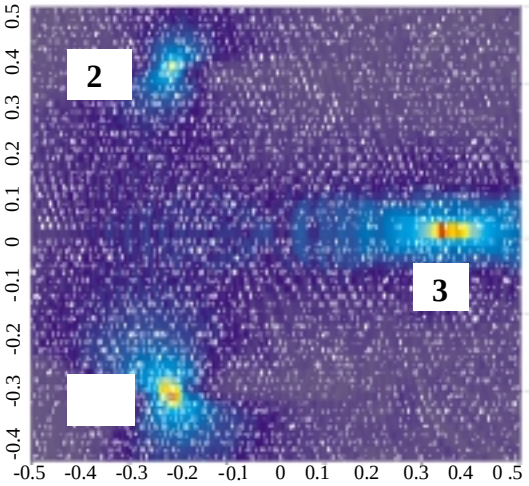

Figure 5.1 Image with proportional intensity.

The phase of the return signal is corrupted by the complex impedance phase of the scatterers. If the type of target is known *a priori,* the complex impedance of the targets' constituent material could be found. Then it is possible to correct the return signals using the average value of the complex phase values of the individual scatterers [17]. This method was found to correct the image reasonably well when the complex impedance phase of the constituent materials has a normal distribution. The average phase value θ_{av} could be found as

$$\theta_{av} = \frac{1}{n} \sum_{i}^{n} \theta_i \tag{5.3}$$

where n is number of different types of complex impedance scatterers and θ_i the complex impedance phase of the i^{th} scatterer. The return signals should be phase corrected by θ_{av}. This mode of correction could be employed in instances where a low chirp rate is used.

6. CONCLUSIONS

Most radar imaging algorithms assume a far field model for the radar back scattered signals. This assumption is valid as long as the target distance from the transceiver is very long. But for a SAR scenario the

near field region is extended beyond the nominal distance and requires focusing. When SAR principle is used for imaging in confined regions, the magnitude of the return signals are also modulated according to the distance. It has been established that the radar scatterers could be modeled by a collection of infinitesimal electric dipoles. Using the exact equations for the scattered electromagnetic field components, it is possible to accurately account for the distance dependence of the magnitude and phase of the reflected signals. Two factors, namely *Magnitude Modifying Factor* and *Phase Modifying Factor*, have been introduced, which describe the magnitude and phase perturbation respectively. Using these two factors a modified near field imaging algorithm has been proposed.

References

1. Stimson, G. W., *Introduction to Airborne Radar,* Hughes Aircraft Co., El Sugundo, CA, 1983.
2. Carrara, W. G., R. S. Goodman, and Majewski, *Spotlight Synthetic Aperture Radar-Signal Processing Algorithms,* Artech House, Boston, 1995.
3. Jakowatz, C. V., *Spotlight mode Synthetic Aperture Radar,* Kluwer Academic Publishers, Boston, 1996.
4. Broquetas, A., J. Palau, L. Jofre, and A. Cardama, "Spherical wave near-field imaging and radar cross-section measurements," *IEEE trans. Antenna and Propagation,* Vol. 46, No. 5, May 1998.
5. Skinner, J. P., B. M. Kent, R. C. Wittmann, D. L. Mensa, and D. J. Andersh, "Normalization and interpretation of radar images," *IEEE trans. Antenna and Propagation,* Vol. 46, No. 4, April 1998.
6. Fitch, P. J., *Synthetic Aperture Radar,* Springer-Verlag, 1988.
7. Kovaly, J. J., *Synthetic Aperture Radar,* Artech House, 1976.
8. Calloway, T. M., C. V. Jakowatz, P. A. Thompson, and P. H. Eichel, "Comparison of synthetic aperture radar autofocus techniques-phase gradient vs subaperture," *SPIE,* Vol. 1566, 1991.
9. Mastin, G. A., S. Plimpton, and D. C. Ghiglia, "Massively parallel synthetic aperture radar autofocus," *SPIE,* Vol. 1566, 1991.
10. Hoole, S. R. H. and P. R. P. Hoole, *Engineering Electromagnetics,* Oxford University Press, Oxford, 1996.
11. Jeng, S. K., "Near-field scattering by physical theory of diffraction and shooting and bouncing rays," *IEEE trans. Antennas and Propagation,* Vol. 46, No. 4, April 1998.

12. Wang, J. H., "An examination of the theory and practices of planar near-field measurements," *IEEE trans. Antennas and Propagation,* Vol. 36, No. 6, June 1988.
13. Gabor, H. T., *Image Reconstruction from Projections: the fundamentals of computerized tomography,* Academic Publishers, San Francisco, 1980.
14. Chen, C. N., and D. I. Hoult, *Biomedical Magnetic Resonance Technology,* AdamHilger, Bristol, New York, 1989.
15. Hedley, M., H. Yan, and D. Rosenfeld, "An improved algorithm for 2-D translational motion artifact correction," *IEEE trans. Med. Imaging,* Vol. 10, No. 4, December 1991.
16. Byron, E., *Radar Principles, Technology, Applications,* Prentice Hall, New Jeresy, 1993.
17. Naveendra, T. S., and P. Hoole, "Complex impedance materials in medical imaging," *Proc. IMRE,* Singapore, March 1998.